Journal of the Optical Society of America B
OPTICAL PHYSICS

Study of a slow-light-enhanced membrane photodetector for realizing on-chip interconnection with low power consumption

Zhichen Gu,[1,*] Takuo Hiratani,[1] Tomohiro Amemiya,[2] Nobuhiko Nishiyama,[1,2] and Shigehisa Arai[1,2]

[1]Department of Electrical and Electronic Engineering, Tokyo Institute of Technology, Meguro, Tokyo 152-8552, Japan
[2]Institute of Innovative Research, Tokyo Institute of Technology, Meguro, Tokyo 152-8552, Japan
*Corresponding author: gu.z.ab@m.titech.ac.jp

Received 13 October 2016; revised 20 December 2016; accepted 21 December 2016; posted 3 January 2017 (Doc. ID 278692); published 26 January 2017

Slow-light propagation can be used to enhance light–matter interactions such as material loss and gain, which enables the realization of ultracompact photonic devices toward the ultralow-power-consumption on-chip or chip-scale optical interconnection. We designed a slow-light-enhanced waveguide-type GaInAs p–i–n photodetector (PD) by using the three-dimensional finite-difference time domain method. As a result, it was found that a cut-off frequency of 19.6 GHz with moderate output voltage, which was attributed to the high impedance characteristic, can be obtained with a 5.5-μm-long PD.

OCIS codes: (050.5298) Photonic crystals; (130.5990) Semiconductors; (200.4650) Optical interconnects; (230.5160) Photodetectors.

https://doi.org/10.1364/JOSAB.34.000440

1. INTRODUCTION

Complementary metal-oxide semiconductor (CMOS) circuits are approaching the limits of their performance. The critical factors hampering further miniaturization of transistors in large-scale integrated circuits (LSIs) are excessive propagation delay and Joule heat generation in electrical interconnects in global wire layers. In recent years, new solutions for interconnecting functional blocks, such as three-dimensional (3D) integrated circuits based on a through-silicon via [1,2], wireless capacitive coupling [3], and inductive coupling [4] have been proposed for overcoming these issues. An on-chip optical interconnection is also considered promising because it can significantly improve the data capacity and power savings relative to copper-based solutions in conventional LSIs [5]. It has been predicted that a data rate over 10 Gb/s and system energy cost much lesser than 100 fJ/bit are required for an on-chip optical interconnection to be competitive with near-future electrical global intrachip interconnects [6]. In this light, our group proposes a monolithic integration platform of membrane photonic devices for realizing an on-chip optical interconnection (Fig. 1). This type of membrane photonic integrated circuit (PIC) can be easily introduced into CMOS LSIs in a back-end-of-line process because it can be bonded onto a Si platform using adhesive or direct bonding technologies [7] instead of by low-temperature direct growth [8]. In terms of the laser source, the membrane structure, which consists of a thin semiconductor core layer sandwiched by low-refractive-index dielectric materials, can provide a significantly high optical confinement factor of the active region and thus enable ultralow threshold current operation. In this case, a lateral-current-injection structure is required for electrical pumping [9]. Furthermore, a surface grating with enhanced index-coupling coefficient by the membrane structure can be introduced in the cladding layer for realizing high-performance membrane distributed-feedback (DFB) [10] or distributed-reflector [11] lasers.

On the other hand, efforts for lowering the energy consumption of opto/electric signal conversion in a membrane PIC are also important. In general, electrical amplifiers such as transimpedance amplifiers (TIAs) and postamplifiers are necessary in an optical receiver for generating a sufficient voltage signal that can be identified by the subsequent electronic circuit with enough bandwidth [12–14]. However, these electrical amplifiers incur an energy cost of the order of pJ/bit level with an assumed data rate of 10 Gb/s; this negates the main advantage of optical interconnection, namely, power saving. This problem can be overcome by combining a photodetector (PD) with a high-load resistor instead of electrical amplifiers, as shown in Fig. 2(a) [15,16]. At the same time, the junction-capacitance $\mathbf{C_j}$ of the p–i–n PD should be extremely small so that a high-level cut-off frequency, which is strongly related to the resistance–capacitance (RC) constant, can be maintained. In addition, the high-load resistor can theoretically lower the thermal noise of

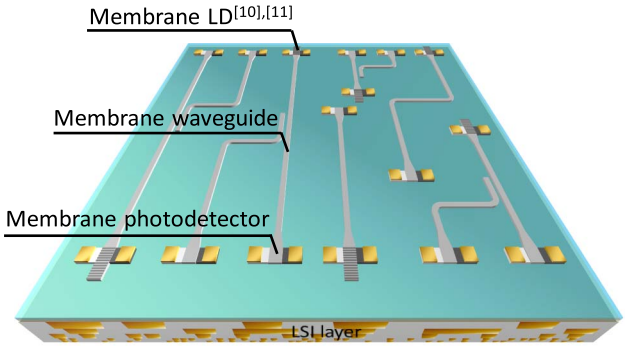

Fig. 1. Concept of a membrane photonic integrated circuit bonded on Si-based CMOS LSI.

the PD and thus increase its sensitivity for realizing error-free operation, which further reduces the overall power consumption of the optical link because the output power required from the laser source can be less. It is estimated that a junction capacitance of less than 1 fF is required for a p–i–n PD to be connected with a load resistor larger than 10 kΩ, providing a cut-off frequency exceeding 10 GHz and an output voltage of several hundred mV with an input light signal of the order of fJ/bit level [17]. Several candidates can realize ultrasmall capacitance owing to their ultracompact size, such as the Ge-waveguide PD [18], nanowire PD [19], and photonic crystal (PhC) PD [20]. Among them, the GaInAs-based PhC-PD is considered the most promising solution owing to its extremely small capacitance of less than 1 fF, high responsivity to 1550-nm wavelength light, and, most importantly, compatibility with membrane PIC that requires a lateral p–i–n junction.

In this work, a slow-light enhanced GaInAs PhC-PD was designed by using the 3D finite-difference time domain (FDTD) method. Unlike in [20], we expected that the PhC [21,22] can significantly reduce the group velocity of the propagation light in the absorption material and thereby reduce the absorption length. We also clarify the coupling structure between the PhC-PD and the input waveguide. Finally, we roughly estimated the bandwidth of the designed structure when it was assumed to be connected by a high-load resistor.

2. DESIGN OF PHC-PD

A. Investigation of Absorption Length

Figure 2(b) shows a conceptual diagram of a slow-light enhanced PD. A GaInAs absorber is assumed to be embedded in the defect region of an air-bridge type InP PhC waveguide, which also forms a lateral p–i–n junction. The PD is considered to be connected with a SiO_2-embedded InP waveguide in consideration of integration with other membrane devices. Note that the fabrication process of such a structure is compatible with the entire membrane optical link, as we have reported before, where a mature etching and regrowth technology will be used for embedding the GaInAs absorber between *p*- and *n*-InP. Air holes will be formed by using 100-kV electron beam (EB) lithography and $CH_4/H_2/Cl_2$ dry etching. Furthermore, an undercut structure can be realized in the last step of the process by using buffered hydrofluoric acid (BHF) wet etching.

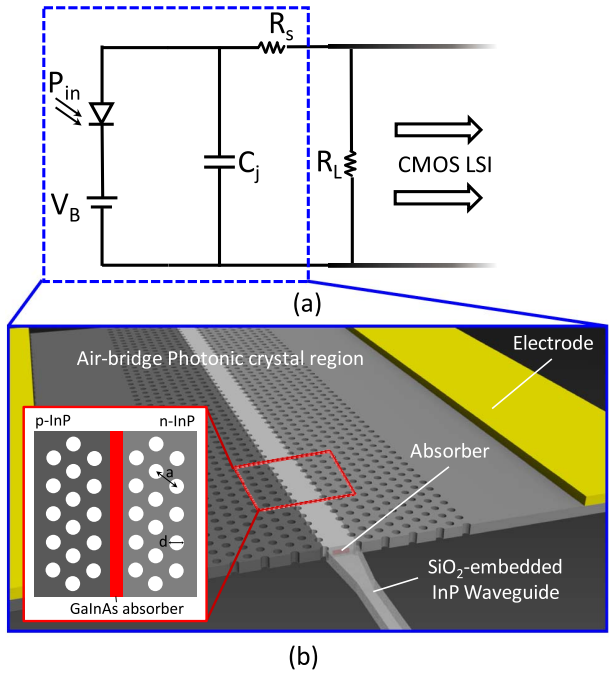

Fig. 2. (a) Equivalent circuit for a p–i–n PD connected by a load resistor, and (b) concept of the GaInAs-based PhC-PD.

Figure 3 shows details of the constructed model for investigating the slow-light effect in the improvement of absorption efficiency. Typical refractive index values of $n_{\mathrm{InP}} = 3.17$ and $n_{\mathrm{GaInAs}} = 3.62$ are adopted in the model, and we assume that the material absorption coefficient of the GaInAs absorber is $\alpha_{\mathrm{GaInAs}} = 5000\ \mathrm{cm}^{-1}$ ($\lambda = 1550$ nm) as a rule of thumb.

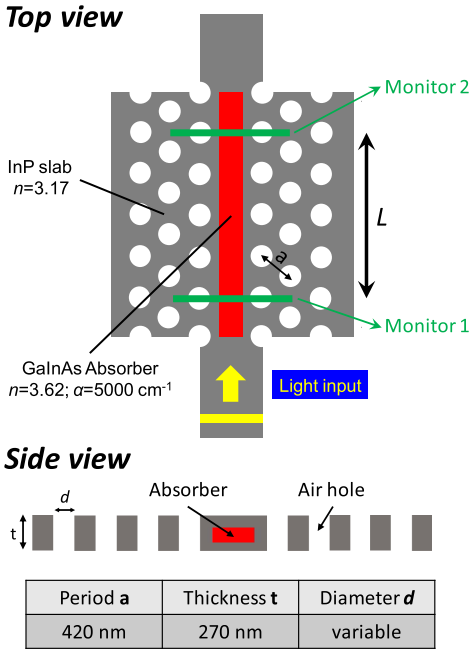

Period **a**	Thickness **t**	Diameter ***d***
420 nm	270 nm	variable

Fig. 3. Top and side views of the calculation model for investigating the relationship between group index and absorption length using the PWE and FDTD methods, respectively.

In consideration of the integration with other membrane devices such as the laser diode and the waveguide, the thickness **t** of the membrane PhC-PD should remain the same as 270 nm, in which an absorber with a 120-nm thickness and 300-nm width is embedded between a 100-nm-thick upper and 50-nm-thick bottom InP cap layer in the vertical direction. The PhC is designed with a fixed lattice constant **a** of 420 nm and an adjustable hole diameter ***d*** for shifting the frequency range of the photonic bandgap (PBG) with a central wavelength near 1550 nm. In terms of the simulation of light propagation in such a structure based on the 3D FDTD method (using a commercial photonic design suite, RSoft), the slow-light enhanced absorption coefficient α_{eff} can be obtained as follows:

$$\alpha_{\mathrm{eff}} = -\frac{\ln(T_2/T_1)}{L}, \tag{1}$$

where T_1 obtained from Monitor 1 is the intensity of the launched continuous-wave light coupled into the absorption region from the input channel waveguide, and T_2, obtained from Monitor 2, is the transmitted intensity after a propagation length of L. Equation (1) assumes that the propagation loss is entirely due to the active material absorption, while it cannot be denied that there must be waveguide scattering loss in such a design. However, it was considered negligible with 10 arrays of air holes on each side of the line defect during the FDTD simulation, for which propagation length is assumed to be extremely short. Theoretically, the modal absorption coefficient, α_{eff}, can be expected to be

$$\alpha_{\mathrm{eff}} = \Gamma \frac{n_g}{n} \alpha_{\mathrm{GaInAs}}, \tag{2}$$

where Γ is the optical confinement factor of the absorber; n_g, the group index; and n, the material index. The well-known slow-down factor $S = n_g/n$ can be expected to proportionally enhance the material absorption per unit length and thereby decrease the absorption length L_a required for obtaining a desired amount of light absorption A, which is set to be 90% in the case of a p–i–n PD:

$$A = 1 - e^{-\alpha_{\mathrm{eff}} L_a} \geq 90\%, \tag{3}$$

under assumption of no scattering loss.

Before investigating L_a and α_{eff}, we used a photonic band solver to calculate the group-index spectrum of the even mode in a GaInAs-embedded line-defect photonic crystal waveguide with different hole diameters based on the plane wave expansion (PWE) method. As shown in Fig. 4, the spectrum will shift to the short-wavelength side with a larger diameter ***d*** because the dielectric contrast is higher, increasing the group index of 1550-nm light from $n_g \approx 9$ in the fast-light regime to $n_g \approx 150$ near the band edge. Regardless of the different ***d*** values, there appears a constant n_g range of ~7 nm in the spectrum, and the corresponding group velocity dispersion (GVD) value β_2 is under 1.5 e^{-20} s^2/m. In terms of the on-chip optical interconnection, a typical spectral width of the 10 Gbps optical signal from the narrow-linewidth DFB laser is far less than this frequency range. Therefore, it is considered that the signal distortion during the optical-to-electronic conversion can be neglected with such low GVD and the extremely short propagation length which equals to the device length of PD.

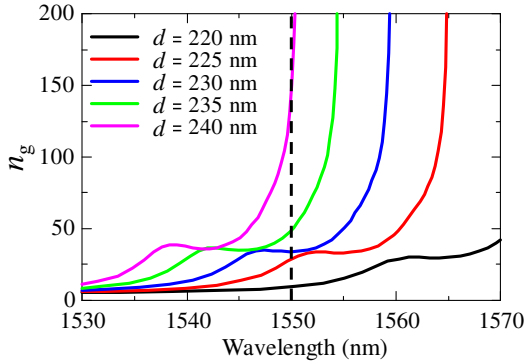

Fig. 4. Calculated group index spectrum for the GaInAs-embedded W1 PhC waveguide with different hole diameters.

An operation wavelength in the precise middle of such a region is preferred in the case of slight variation of the lasing wavelength of the membrane laser diode.

Figure 5(a) shows the calculated modal absorption coefficient based on the FDTD method and the corresponding absorption length for realizing 90% light absorption according to Eq. (3). α_{eff} varies from 3190 to 9150 cm^{-1} with increasing ***d*** or n_g. For comparison with the theoretical value derived using Eq. (2), Γ of the absorber is calculated by setting two total energy density volume monitors in the PhC waveguide during the FDTD simulation. The obtained results, shown in Fig. 5(b), indicate that the drastic interference of light multiscattering induced by larger hole diameter ***d*** would reduce the group velocity of the propagating light and cause an expansion of the mode field in the lateral direction, thereby reducing Γ of the absorber from 0.32 to 0.22. There is a trade-off between the slow-light effect and the optical confinement, whereas in our case, it can

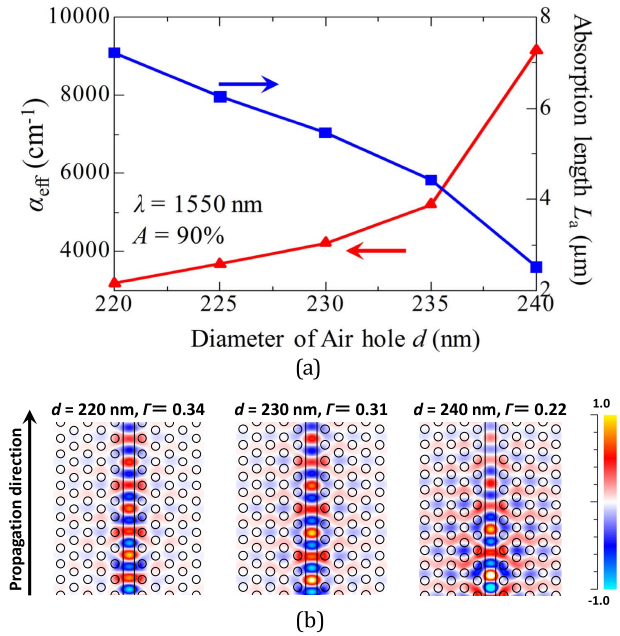

Fig. 5. (a) FDTD simulation result of slow-light enhanced absorption coefficient α_{eff} and corresponding absorption length L_a. (b) The corresponding mode field distribution for d = 220, 230, and 240 nm.

be said that the significantly increased group index still dominantly influences the enhancement of α_{eff}. However, it is clear that the FDTD simulation result is far less than the theoretical value. In other words, in theory, α_{eff} should be larger than 16000 cm^{-1} with $n_g = 35$, $n = 3.17$, and $\Gamma = 0.30$ when $d = 230$ nm. The strongly mismatched result can be explained by the following two numerical analyses [23–25]. First, the PWE method can only deal with a Hermitian eigenproblem converted from Maxwell's equations, which means that the dielectric constant ϵ of the media in the calculation model should be purely real (lossless). Therefore, the presence of the absorption coefficient of the GaInAs absorber has not been considered during the calculation of the PBG based on PWE, which would cause a "smearing" effect of the photonic density of states—the destructive interference of the multiply scattered wave becomes incomplete and the group index no longer diverges when approaching the band edge. Consequently, there would be a drastic reduction of n_g near the band edge and a modest reduction of n_g within the entire defect band. Second, it is predicted that a hybridization of the propagation modes and evanescent modes in the waveguide would be induced if the material absorption loss exceeds a certain value, which may substantially weaken the slow-light effect and thus lead to an associated saturation of the attainable absorption. These two analyses well explain the drastic reduction of the desired slow-light enhancement of the absorption considering that the absorption coefficient α_{eff} of the GaInAs absorber is very large. Nevertheless, this slow-light effect is still attractable even in the presence of relatively high loss. An extremely short length of 2.5 μm can be expected for realizing 90% absorption efficiency with the highest attainable group index near the band edge when $d = 240$ nm. However, we considered $d = 230$ nm a better choice because of the tolerance of the manufacturing error of the air hole diameter and the variation of the operation wavelength, as mentioned before. In this case, a low GVD region with central wavelength of 1550 nm can be obtained with the thickness $t = 270$ nm and period $a = 420$ nm. And the absorption length L_a would be 5.5 μm with a relatively modest group index $n_g \sim 35$, which is the half-length of a conventional waveguide-type PD based on the current membrane layer structure.

B. Coupling Structure between PhC-PD and Channel Waveguide

Efficient coupling of guided light from a channel waveguide into a slow-light regime PhC waveguide is known to be challenging owing to the different structure of conventional index guiding and PBG guiding, which causes mismatch in the mode field overlap and group velocity. In our case, the overall absorption efficiency of the PhC-PD could be reduced undesirably owing to the nonnegligible reflection and scattering during the coupling process, and therefore, an efficient coupling structure design is required. In recent decades, many schemes have been proposed for addressing this coupling issue. Vlasov and McNab mentioned the importance of optimizing the termination of PhCs at the coupling interface, which helps improve efficiency by creating appropriate photonic surface states [26]. Yang *et al.* extended this idea and achieved a further improvement by using topology optimization [27]. Other solutions of adiabatic tapers, such as introducing additional holes at the interface [28], using width-modulated PhC waveguides [29], introducing fast-light sections between the channel waveguide and slow-light region that allows Bloch modes to build up [30], or tapering the size or period of the air hole at the entrance of PhC waveguide [31], have also been analyzed theoretically or demonstrated experimentally. Among them, the air-wedge coupling structure is considered most attractive because it can provide highly efficient wideband group velocity independent coupling with a relatively smaller taper region compared to other works [32]. Furthermore, it has been proved that the designed structure would be robust to any fabrication imperfections.

Figure 6 shows a schematic figure of an air-wedge coupler introduced in our design of the PhC-PD. A SiO_2-cladding InP channel waveguide, which provides more mechanical stability than the air-bridge channel waveguide, is used for connecting the taper and other membrane components in the integrated circuit (point A). At the end of the taper region, the channel waveguide is joined to the PhC waveguide right at the center of the air holes as an optimized termination (point B). The mode from the channel waveguide is transformed smoothly into the GaInAs-embedded PhC waveguide by gradually replacing the channel waveguide structure with air holes and thereby linearly extending the evanescent mode field. The coupling loss at point A is less than 0.02 dB according to the calculation result based on the finite-difference method, which is considered to be a negligible value when investigating the coupling loss between the channel waveguide and the PhC waveguide. The loss at point B is supposed to be suppressed by adjusting the width and length of the air-wedge region, indicated as h_x and h_y in the figure. It should be noted that the target wavelength is set to 1550 nm during the simulation, which is the same as in the analysis of the absorption length in the previous section. According to the mode field shown in Fig. 5(b), a taper width h_x larger than $2\sqrt{3}a$ is required for making the evanescent field amplitude of the Bloch mode significantly decayed at the start point A and thereby eliminate the discontinuity between the

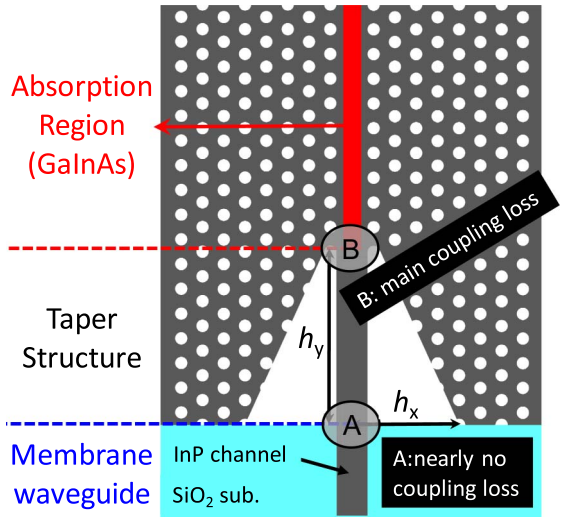

Fig. 6. Top view of the introduced air-wedge structure for improving the coupling efficiency between the PhC-PD and channel waveguide.

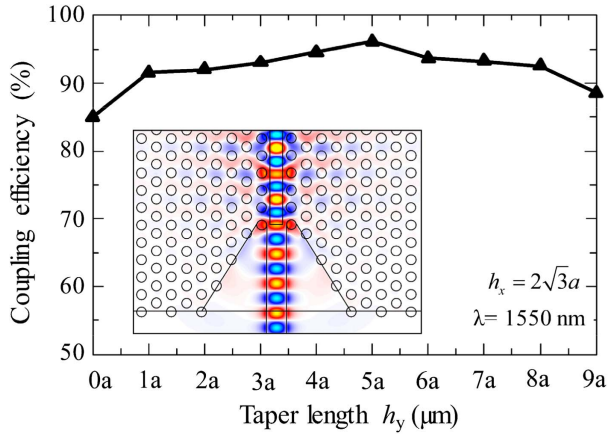

Fig. 7. Calculation result of coupling efficiency of the operation wavelength of 1550 nm with fixed h_x and varying h_y.

channel waveguide mode and PhC waveguide mode at lower group velocity. Figure 7 shows the transmission characteristic of the air-wedge coupler with fixed h_x and varying taper length h_y. We can see that the maximum coupling efficiency η_c of 96% can be obtained at a fixed operation wavelength when $h_x = 2\sqrt{3}a$ and $h_y = 5a$, as shown in the embedded figure of the mode field distribution. At the same time, the reflected light was found to be lower than −35 dB by placing a power monitor behind the incident point of light. Based on the former calculation, the responsivity R of the designed PD can be expected to be larger than 1 A/W according to Eq. (4):

$$R = \eta_c \cdot \frac{e}{h\nu} \cdot A. \tag{4}$$

However, in reality, R suffers from propagation loss owing to the PhC imperfection or nonradiative carrier recombination loss at the heterojunction interface. It is difficult to consider these two issues at the design stage, and we believe that the latest regrowth and fabrication technology can make them less important.

3. ESTIMATION OF 3-DB BANDWIDTH

The cut-off frequency $f_{3\,\mathrm{dB}}$ of our PhC-PD has been estimated after analyzing the device structure to ensure that it can match the modulation speed of the membrane laser when connected to an extremely high load resistor for realizing sufficient voltage output. In terms of the high-frequency response, the 3-dB bandwidth of the lateral junction p–i–n PD is limited by the carrier drift time within the intrinsic region and resistance-capacitance delay that correspond to the transit frequency f_{TT} and RC bandwidth f_{RC}, as shown in Eq. (5). Obviously, a maximum $f_{3\,\mathrm{dB}}$ can be achieved when both frequencies are equal [33]:

$$\frac{1}{f_{3\,\mathrm{dB}}^2} = \frac{1}{f_{\mathrm{RC}}^2} + \frac{1}{f_{\mathrm{TT}}^2}. \tag{5}$$

Specifically, f_{RC} can be described by Eq. (6) as follows:

$$f_{\mathrm{RC}} = \frac{1}{2\pi(R_{\mathrm{L}} + R_{\mathrm{s}})C_{\mathrm{j}}}, \tag{6}$$

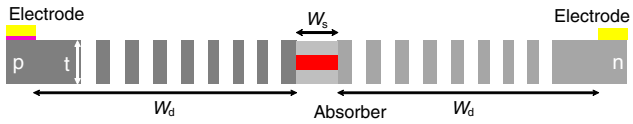

Fig. 8. Enlarged cross-sectional view of the calculation modal of $f_{3\,\mathrm{dB}}$.

where R_{L} and R_{s} are the load resistor and sheet resistance of the PhC-PD, as indicated in the equivalent circuit in Fig. 2(a). As seen in the enlarged cross-sectional calculation model in Fig. 8, the junction capacitance C_{j} of the designed PD can be roughly estimated to be 0.6 fF by applying the width W_{s} of the GaInAs absorber (intrinsic region), thickness t of the InP slab, and designed absorption length L into the parallel plate model, which was less than the target of 1 fF as mentioned in Section 1. R_{L} is assumed to be 10 kΩ during the estimation for providing a sufficient output voltage to the CMOS circuit. R_{s} is strongly related to the distance W_{d} between the absorber and the electrodes. A small array of air holes is preferred for reducing R_{s}; at the same time, it should be able to provide enough structure dispersion and lateral optical confinement in plane. According to the FDTD calculation result shown in Fig. 9, which gives the relationship between the scattering loss and the number of

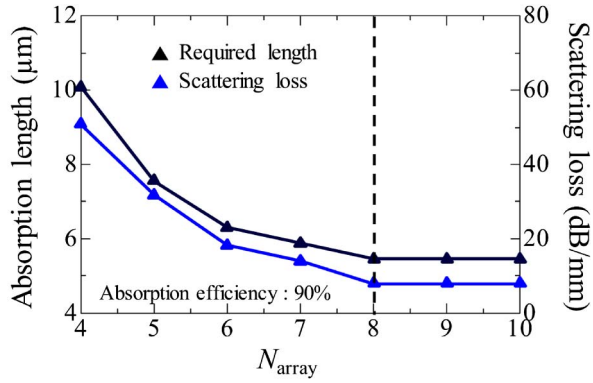

Fig. 9. Dependence of number of arrays of air holes on scattering loss and device length.

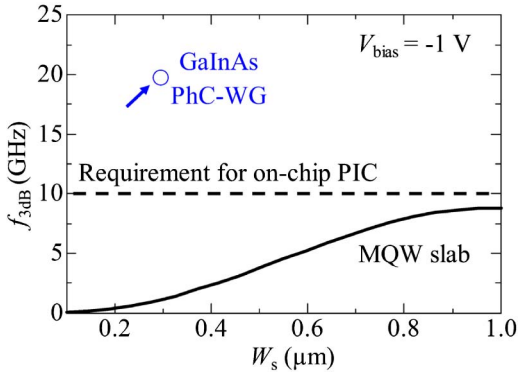

Fig. 10. Comparison of the estimated 3-dB bandwidth of the designed PhC-PD and the reported MQW-absorber-based waveguide-type PD.

Table 1. Comparison with Recent Researches of Ultra-Compact PDs

Device Structure	Absorption Length (μm)	Absorption Volume (μm3)	V_{bias} (V)	DC Response (A/W)	3-dB Bandwidth (GHz)	Ref.
Si-Plasmonic[a,c]	5.0	0.11	−3.25	0.126	40 w/o R_L	[36]
InGaAs-Plasmonic[b,d]	Periodic	0.02/unit	3.0	0.74	140 w/o R_L	[37]
InAsSb-Nanowire[b,d]	Periodic	0.03/unit	0.15	0.3	–	[38]
Si-Graphene[a,c]	40.0	0.01	−3.2	0.36	42 w/o R_L	[39]
Ge-Waveguide[a,c]	13.8	2.76	−1.0	1.0	28 w/o R_L	[40]
InGaAs/Si Hybrid[a,d]	30	-	−3.0	0.95	30 w/o R_L	[41]
This work[a,d]	5.5	0.45	−1.0	1.0	19.6 w/ $R_L = 10$ kΩ	

[a]In-plane.
[b]Vertical illumination.
[c]Experimental data.
[d]Simulation data.

arrays of air holes by adding two power monitors on both left and right side of the PhC waveguides, at least eight arrays of air holes are required for suppressing the scattering loss and thereby increasing the corresponding absorption length for ensuring an absorption efficiency of 90%, which means that W_d should be larger than 3 μm with a fixed lattice constant **a** of 420 nm. On the other hand, f_{TT} can be obtained by the following equation [34]:

$$f_{TT} = \frac{\sqrt{2}}{\pi} \frac{v_{sat} \cdot \tanh\left(\mu_h \cdot \frac{V_{bias}}{W_s} \cdot \frac{1}{v_{sat}}\right)}{W_s}, \tag{7}$$

where v_{sat} is the hole saturation drift velocity; μ_h, its mobility; and V_{bias}, the assumed applied bias voltage of −1 V in consideration of the supply voltage of the recent CMOS LSI. Obviously, f_{TT} can also be determined by the fixed W_s. Based on all the parameters and equations mentioned previously, the 3-dB bandwidth of our PhC-PD can be expected to be 19.6 GHz, which is a significantly improved value compared to the reported multi-quantum-well (MQW)-absorber-based waveguide-type PD [35], and this is more than sufficient for the high-speed on-chip optical interconnection, as shown in Fig. 10. In addition, simulation and experimental results of recent researches of ultracompact PDs toward optical interconnection are listed in Table 1 for comparison. As shown, our design can provide both high responsivity and sufficient speed with an ultrasmall size. Also, the power consumption of the designed ampless PD can be expressed by the product of the reverse bias and the photocurrent divided by the data rate of the optical signal. A photocurrent of a few tens of μA will be enough for providing a sufficient output voltage of several hundreds of mV with a high load resistor of 10 kΩ. Therefore, the power consumption will be only several fJ/bit with a signal rate of larger than 10 Gb/s in the on-chip optical interconnection, which is a value far less than is the case of for a conventional PD-TIA.

4. CONCLUSION

A detailed design for an ultracompact PhC GaInAs p–i–n-PD based on the slow-light effect was provided for realizing an on-chip optical interconnection with ultralow power consumption. By using the PWE and FDTD solver supported by a commercial photonic design suite, an absorption length of only 5.5 μm can be expected for realizing an absorption efficiency of 90% with a relatively modest group index of ∼35 at a fixed operation wavelength of 1550 nm. An air-wedge structure is adopted in the design for improving the coupling efficiency between the PhC-PD and the channel waveguide, which can be expected to exceed 96% with a suitable design. The 3-dB bandwidth of the designed PhC-PD is estimated to be 19.6 GHz even when it is connected with an extremely high load resistor of 10 kΩ, and therefore, a sufficient voltage output can be obtained for driving the subsequent electronics in CMOS circuits.

Funding. Japan Society for the Promotion of Science (JSPS) (15H05763, 15J04654, 15J11776, 16H06082, 16J11581, 25709026).

REFERENCES

1. M. Kada, "Development of functionally innovative 3D-integrated circuit (dream chip) technology/high-density 3D-integration technology for multifunctional devices," in *IEEE International Conference on 3D System Integration (3DIC)* (IEEE, 2009), pp. 1–6.
2. V. Suntharalingam, R. Berger, S. Clark, J. Knecht, A. Messier, K. Newcomb, D. Rathman, R. Slattery, A. Soares, C. Stevenson, K. Warner, D. Young, L.-P. Ang, B. Mansoorian, and D. Shaver, "A four-side tileable back illuminated, three-dimensionally integrated megapixel CMOS image sensor," in *IEEE Solid-State Circuits Conference Digest of Technical Papers (ISSCC)* (IEEE, 2009), pp. 38–39.
3. A. Fazzi, R. Bologna Canegallo, L. Ciccarelli, L. Magagni, F. Natali, E. Jung, P. Rolandi, and R. Guerrieri, "3-D capacitive interconnections with mono-and bi-directional capabilities," IEEE J. Solid-State Circuits **43**, 275–284 (2008).
4. K. Niitsu, Y. Shimazaki, Y. Sugimori, Y. Kohama, K. Kasuga, I. Nonomura, M. Saen, S. Komatsu, K. Osada, N. Irie, T. Hattori, A. Hasegawa, and T. Kuroda, "An inductive-coupling link for 3D integration of a 90 nm CMOS processor and a 65 nm CMOS SRAM," in *IEEE Solid-State Circuits Conference Digest of Technical Papers (ISSCC)* (IEEE, 2009), pp. 480–481.
5. M. Haurylau, G. Chen, H. Chen, J. Zhang, N. A. Nelson, D. H. Albonesi, E. G. Friedman, and P. M. Fauchet, "On-chip optical interconnect roadmap: challenges and critical directions," IEEE J. Sel. Top. Quantum Electron. **12**, 1699–1705 (2006).
6. D. A. B. Miller, "Device requirements for optical interconnects to silicon chips," Proc. IEEE **97**, 1166–1185 (2009).
7. S. Arai, N. Nishiyama, T. Maruyama, and T. Okumura, "GaInAsP/InP membrane lasers for optical interconnects," IEEE J. Sel. Top. Quantum Electron. **17**, 1381–1389 (2011).
8. R. Chen, K. W. Ng, W. S. Ko, D. Parekh, F. Lu, T. D. Tran, K. Li, and C. Chang-Hasnain, "Nanophotonic integrated circuits from nanoresonators grown on silicon," Nat. Commun. **5**, 4325 (2014).

9. D. Inoue, J. Lee, K. Doi, T. Hiratani, Y. Atsuji, T. Amemiya, N. Nishiyama, and S. Arai, "Room-temperature continuous-wave operation of GaInAsP/InP lateral-current-injection membrane laser bonded on Si substrate," Appl. Phys. Express **7**, 072701 (2014).
10. D. Inoue, T. Hiratani, K. Fukuda, T. Tomiyasu, T. Amemiya, N. Nishiyama, and S. Arai, "High-modulation efficiency operation of GaInAsP/InP membrane distributed feedback laser on Si substrate," Opt. Express **23**, 29024–29031 (2015).
11. T. Hiratani, D. Inoue, T. Tomiyasu, Y. Atsuji, K. Fukuda, T. Amemiya, N. Nishiyama, and S. Arai, "Room-temperature continuous-wave operation of membrane distributed-reflector laser," Appl. Phys. Express **8**, 112701 (2015).
12. W. Chen, Y. Cheng, and D. Lin, "A 1.8-V 10-Gb/s fully integrated CMOS optical receiver analog front-end," IEEE J. Solid-State Circuits **40**, 1388–1396 (2005).
13. J. E. Proesel, B. G. Lee, A. V. Rylyakov, C. W. Baks, and C. L. Schow, "Ultra-low-power 10 to 28.5 Gb/s CMOS-driven VCSEL-based optical links [Invited]," J. Opt. Commun. Netw. **4**, B114–B123 (2012).
14. J. Kim and J. F. Buckwalter, "A 40-Gb/s optical transceiver front-end in 45 nm SOI CMOS," IEEE J. Solid-State Circuits **47**, 615–626 (2012).
15. C. Debaes, A. Bhatnagar, D. Agarwal, R. Chen, G. A. Keeler, N. C. Helman, H. Thiennpont, and D. A. B. Miller, "Receiver-less optical clock injection for clock distribution networks," IEEE J. Sel. Top. Quantum Electron. **9**, 400–409 (2003).
16. S. Assefa, F. Xia, M. J. Green, C. L. Schow, and Y. A. Vlasov, "CMOS-integrated optical receivers for on-chip interconnects," IEEE J. Sel. Top. Quantum Electron. **16**, 1376–1385 (2010).
17. K. Nozaki, S. Matsuo, K. Takeda, T. Sato, E. Kuramochi, and M. Notomi, "InGaAs nano-photodetectors based on photonic crystal waveguide including ultracompact buried heterostructure," Opt. Express **21**, 19022–19028 (2013).
18. C. T. DeRose, D. C. Trotter, W. A. Zortman, A. L. Starbuck, M. Fisher, M. R. Watts, and P. S. Davids, "Ultra compact 45 GHz CMOS compatible germanium waveguide photodiode with low dark current," Opt. Express **19**, 24897–24904 (2011).
19. M. L. Brongersma, L. Y. Cao, J. S. Park, P. Y. Fan, and B. Clemens, "Resonant germanium nanoantenna photodetectors," Nano Lett. **10**, 1229–1233 (2010).
20. K. Nozaki, S. Matsuo, T. Fujii, K. Takeda, M. Ono, A. Shakoor, E. Kuramochi, and M. Notomi, "Photonic-crystal nano-photodetector with ultrasmall capacitance for on-chip light-to-voltage conversion without an amplifier," Optica **3**, 483–492 (2016).
21. T. Baba, "Slow light in photonic crystals," Nat. Photonics **2**, 465–473 (2008).
22. J. Fu, A. Tandaechanurat, S. Iwamoto, and Y. Arakawa, "Design of large-bandwidth single-mode operation waveguides in silicon three-dimensional photonic crystals using two guided modes," Opt. Express **21**, 12443–12450 (2013).
23. J. G. Pedersen, S. Xiao, and N. A. Mortensen, "Limits of slow light in photonic crystals," Phys. Rev. B **78**, 153101 (2008).
24. J. Grgic, J. R. Ott, F. Wang, O. Sigmund, A.-P. Jauho, J. Mork, and N. A. Mortensen, "Fundamental limitations to gain enhancement in periodic media and waveguides," Phys. Rev. Lett. **108**, 183903 (2012).
25. T. P. White and A. A. Sukhorukov, "Transition from slow and frozen to superluminal and backward light through loss or gain in dispersion-engineered waveguides," Phys. Rev. A **85**, 043819 (2012).
26. Y. Vlasov and S. McNab, "Coupling into the slow light mode in slab-type photonic crystal waveguides," Opt. Lett. **31**, 50–52 (2006).
27. L. Yang, A. V. Lavrinenko, L. H. Frandsen, P. I. Borel, A. Têtu, and J. Fage-Pedersen, "Topology optimisation of slow light coupling to photonic crystal waveguides," Electron. Lett. **43**, 923–924 (2007).
28. P. Sanchis, J. Marti, A. Garcia, A. Martinez, and J. Blasco, "High efficiency coupling technique for planar photonic crystal waveguides," Electron. Lett. **38**, 961–962 (2002).
29. P. Pottier, M. Gnan, and R. Rue, "Efficient coupling into slow-light photonic crystal channel guides using photonic crystal tapers," Opt. Express **15**, 6569–6571 (2007).
30. J. P. Hugonin, P. Lalanne, T. P. White, and T. F. Krauss, "Coupling into slow-mode photonic crystal waveguides," Opt. Lett. **32**, 2638–2640 (2007).
31. C. Lin, X. Wang, S. Chakravarty, B. Lee, W. Lai, and R. T. Chen, "Wideband group velocity independent coupling into slow light silicon photonic crystal waveguide," Appl. Phys. Lett. **97**, 183302 (2010).
32. M. Askari and A. Adibi, "High efficiency coupling of light from a ridge to a photonic crystal waveguide," Appl. Opt. **52**, 5803–5815 (2013).
33. S. Klinger, M. Berroth, M. Kaschel, M. Oehme, and E. Kasper, "Ge-on-Si p-i-n photodiodes with a 3-dB bandwidth of 49 GHz," IEEE Photon. Technol. Lett. **21**, 920–922 (2009).
34. J. Pereira, "Modeling the frequency response of p^+InP/n^-InGaAs/n^+InP photodiodes with an arbitrary electric field profile," COMPEL **26**, 1114–1122 (2007).
35. D. Inoue, T. Hiratani, Y. Atsudi, T. Tomiyasu, T. Amemiya, N. Nishiyama, and S. Arai, "Monolithic integration of membrane-based butt-jointed built-in DFB lasers and PIN photodiodes bonded on Si substrate," IEEE J. Sel. Top. Quantum Electron. **21**, 1502907 (2015).
36. S. Muehlbrandt, A. Melikyan, T. Harter, K. Kohnle, A. Muslija, P. Vincze, S. Wolf, P. Jakobs, Y. Fedoryshyn, W. Freude, J. Leuthold, C. Koos, and M. Kohl, "Silicon-plasmonic internal-photoemission detector for 40 Gbit/s data reception," Optica **3**, 741–747 (2016).
37. J. Guo, Z. Wu, Y. Li, and Y. Zhao, "Design of plasmonic photodetector with high absorptance and nano-scale active regions," Opt. Express **24**, 18229–18242 (2016).
38. W. Lee, P. Senanayake, A. Farrell, A. Lin, C. Hung, and D. Huffaker, "High quantum efficiency nanopillar photodiodes overcoming the diffraction limit of light," Nano Lett. **16**, 199–204 (2016).
39. R. Shiue, Y. Gao, Y. Wang, C. Peng, A. D. Robertson, D. K. Efetov, S. Assfa, F. H. L. Koppens, J. Hone, and D. Englund, "High-responsivity graphene-boron nitride photodetector and autocorrelator in a silicon photonic integrated circuit," Nano Lett. **15**, 7288–7293 (2015).
40. H. Chen, P. Verheyen, P. D. Heyn, G. Lepage, J. D. Coster, P. Absil, G. Roelkens, and J. V. Campenhout, "High-responsivity low-voltage 28-Gb/s Ge p-i-n photodetector with silicon contacts," J. Lightwave Technol. **33**, 820–824 (2015).
41. D. Yin, T. He, Q. Han, Q. Lv, Y. Zhang, and X. Yang, "High-responsivity 40 Gbit/s InGaAs/InP PIN photodetectors integrated on silicon-on-insulator waveguide circuits," J. Semicond. **37**, 114006 (2016).